BMC Cancer

RESEARCH

Open Access

TRPM2 channels mediate ROS-induced actin remodeling and cell migration of prostate cancer cells

Pengwei Qi[1†], Jingting Zhao[1†], Hongtian Zhang[1†], Xingyu Liu[2], Qing You[3], Jianguo Niu[3], Xiangming Ye[1*] and Fangfang Li[1*]

Abstract

Background Actin remodeling plays important roles in pathophysiological processes such as cancer metastasis and angiogenesis. Reactive oxygen species (ROS) are signaling molecules thought to regulate cell migration by remodeling actin cytoskeleton. Earlier, we demonstrated that Transient receptor potential melastatin 2 (TRPM2) channels mediates H_2O_2-induced actin remodeling and cell migration in HeLa cells by manipulating Ca^{2+} and Zn^{2+}. However, the mechanism by which ROS produced in models more relevant to pathophysiological circumstances affect the actin cytoskeleton, remains poorly unknown. Therefore, this study aimed to explore the effect of ROS produced from pathophysiological conditions on actin cytoskeleton and cell migration. And then investigates the role of TRPM2 channels in the regulation of these types of ROS-induced actin remodeling and cell migration in prostate cancer cells.

Methods The study utilized various molecular probes, reagents, and cell culture techniques. Prostate cancer (PC)-3 and DU145 cell line were cultured and treated with different compounds to induce ROS production and actin remodeling. The actin cytoskeleton was stained with phalloidin or labelled with pActin-tdTomato plasmid and imaged using confocal microscopy. Zn^{2+} and Ca^{2+} levels were measured by Fluozin3-AM and Fluo4-AM probes respectively. Cell migration as-says were performed to assess the role of TRPM2 channels.

Results We demonstrated that both H_2O_2 and palmitate induces TRPM2-dependent elevation of cytosolic Ca^{2+} and Zn^{2+}, leading to actin remodeling both in PC-3 and DU145 cells. Inhibition or knockdown of TRPM2 channels or chelation of Zn^{2+} significantly reduced these effects.

Conclusions TRPM2 channels and TRPM2-mediated Zn^{2+} are essential in ROS-induced actin remodeling and cell migration in prostate cancer cells. Preventing TRPM2 channel activation and chelating Zn^{2+} may offer potential therapeutic strategies for preventing cancer metastasis. Further research is needed to identify molecular targets of Zn^{2+} in the actin cytoskeleton and cancer cell migration.

Keywords ROS, TRPM2 channel, Ca^{2+}, Zn^{2+}, Actin remodeling, Cell migration

†Pengwei Qi, Jingting Zhao and Hongtian Zhang contributed equally to this work.

*Correspondence:
Xiangming Ye
yexiangming@hmc.edu.cn
Fangfang Li
fangfangli722@163.com
Full list of author information is available at the end of the article

Introduction

Cell migration plays a crucial role in multiple processes such as tumor cell invasion, wound healing and immune responses [1, 2]. During migration, cells undergo constant remodeling of the cytoskeleton into filopodia, lamellipodia and stress fibers [3–6]. Filopodia are hairlike membrane protrusions where actin fibers are arranged into parallel bundles [4]. Lamellipodia are characterized by a dense network of actin filaments formed at the leading edge of migrating cells, where actin polymerases into a cortical ring [5]. Stress fibers are contractile filament bundles linked by α-actinin and myosin [6]. A variety of factors regulating dynamics of actin cytoskeleton have been proposed [7], of which reactive oxygen species (ROS) [8, 9] and Ca^{2+} signaling [10, 11] are noteworthy.

The generation of ROS is inevitable for carcinoma cells in cancer microenvironment. Epidermal Growth Factor (EGF), a well-known growth factor, has been demonstrated to mediate ROS production to enhance cancer cell migration [12, 13]. Besides, the free saturated fatty acid, palmitate, could promote the generation of ROS to induce cell migration [14]. Therefore, ROS may represent the key factor linking dysregulated metabolism and cancer pathogenesis. And it has been demonstrated that the 'non-damaging' levels of ROS could promote signal transduction to mediate cellular processes, such as actin remodeling [15, 16] and cell migration [17], rather than causing a deleterious effect. Despite dysregulated fatty acid metabolism is correlated with pathogenesis of cancers [18], the precise underlying mechanism remains unclear.

Multiple studies have demonstrated that Ca^{2+} regulates cell migration through spatial and temporal regulation of the actin cytoskeleton. For example, Tsai et al. reported that elevating cytosolic Ca^{2+} level decreases cell migration in both endothelial and lung carcinoma cells [19]. While, a recent study demonstrated that the plasma membrane Ca^{2+} ATPase (PMCA) 4b inhibits migration and metastasis of BRAF mutant melanoma cells by perturbing cytoskeleton reorganization, besides, this study reported that the PMCA4b expressing A375 cells maintained front-to-rear Ca^{2+} concentration gradient to preserve lamellipodia and stress fibre formation [20].

Since TRPM2 channels are highly sensitive to ROS and permeable to Ca^{2+} [21, 22], it was hypothesized that TRPM2 channels mediate the effects of ROS on cell migration by remodeling the actin cytoskeleton. To address this, the role of TRPM2 channels in ROS-mediated actin remodeling and cell migration was investigated in this study. PC-3 cell line was chosen. PC-3 is a cell line derived from human prostate cancer. Our results demonstrate that TRPM2 channels indeed mediate actin remodeling and cell migration induced by different types of ROS (H_2O_2 or generated upon palmitate treatment). We found that ROS-mediated activation of TRPM2 channels raises both the cytosolic level of free Ca^{2+} and Zn^{2+}, with Zn^{2+} playing a dominant role in actin remodeling and cell migration.

Materials and methods

Molecular probes and reagents

LysoTracker Red (L7528), MitoTracker Red (M7512) and ER-tracker Red (E34250), Alexa-Fluor-488- conjugated phalloidin(A12379), Pluronic F127 (P6866), Fura-2-AM (F1221), Fluo-4-AM (F14217), FluoZin-3-AM (F24195) and SuperScript ii reverse transcriptase (18064071) were purchased from Thermo Fisher Scientific. Palmitic Acid (HY-N0830), ACA (HY-118628), NAC (HY-B0215), Clotrimazole (HY-10882), BAPTA-AM (HY-100545), TPEN (HY-100202), Econazole (HY-B0885), Zinc Pyrithione (HY-B0572), A23187 (HY-N6687), CASIN (HY-12874), NSC 23766 (HY-15723) were from MedChemExpress. As palmitic acid is insoluble in water, it is commonly conjugated to fatty acid-free bovine serum albumin (BSA, Beyotime, ST025) as previously described [23]. Briefly, Palmitate-BSA complex (stock) was prepared by mixing 100 mM palmitic acid (made up in ethanol) with 10% BSA at 50 °C and stored at 4 °C.

Antibodies and plasmid

For western blot, TRPM2 Rabbit Polyclonal Antibody (Catalog# HA500437, HUABIO, 1:1000) was used as primary antibody and HRP-conjugated Goat anti-Rabbit IgG polyclonal antibody (Catalog# HA1001, HUABIO, 1:50,000) was used as secondary antibody. Lifeact-mCherry plasmid was kindly provided by Prof. Wei Yang (Department of Biophysics, Zhejiang University School of Medicine, Hangzhou, China).

Cell culture

PC-3 cells used in this study were cultured in RPMI-1640 with GlutaMAX™ medium (Thermo Fisher Scientific, 61870036) supplemented with 10% fetal bovine serum (Noverse, NFBS-2500 A) and 1% streptomycin/penicillin (Yeasen, 60162ES76). DU145 cells used in this study were cultured in MEM α (Thermo Fisher Scientific, 12571063) supplemented with 10% fetal bovine serum (Noverse, NFBS-2500 A) and 1% streptomycin/penicillin (Yeasen, 60162ES76). Cells were cultured at 37 °C under 5% CO_2 humidified conditions.

RNAi

Control siRNA, TRPM2-siRNA-1, and TRPM2-siRNA-2 were obtained from GenePharma and transfected into indicated cells using Lipofectamine RNA iMAX (Thermo Fisher Scientific, 13778500) according to the

manufacturer's instructions. The sequences are as follows: control siRNA sense (50 -UUCUCCGAACGU GUCACGUTT-30) and antisense (50 -ACGUGACAC GUUCGGAGAATT-30); TRPM2-siRNA-1 sense (50—CGGAGUUCCUGAUCUAUGATT-30) and antisense (50 -UCAUAGAUCAGGAACUCCGTT-30); TRPM2-siRNA-2 sense (50 -GUGGGACCCAAAGAAACAUTT-30) and antisense (50 -AUGUUUCUUUGGGUCCCA CTT-30).

Western blot

Whole cell proteins were isolated using RIPA Lysis Buffer (Beyotime, P0013B) with protease and phosphatase inhibitor cocktail (Beyotime, P1005) on ice for 30 min. After centrifugation at 12,000 g for 10 min at 4℃, the supernatants were collected and quantified using bicinchoninic acid assay (BCA; Thermo Fisher Scientific, 23225). The 20 µg proteins were separated by 10%SDS-PAGE and electroblotted onto 0.22-µm PVDF membranes (Millipore, Sigma). Following blocking by TBST containing 5% skim milk for 1 h, the membrane was incubated overnight at 4℃ with TRPM2 Rabbit Polyclonal Antibody (1:1000). After incubation with peroxidase-conjugated secondary antibody (1:50,000) for 1 h at room temperature, the signals were visualized using enhanced chemiluminescence (Med Chem Express, HY-K2005). Blots were analyzed using the ChemiDoc Touch Imaging System (Bio-Rad) and Image Lab Software (Bio-Rad).

qRT-PCR

Total RNA was extracted using a RNeasy Plus Micro Kit (QIAGEN, 74034) according to the manufacturer's instructions. cDNA was synthesized from 1 µg of total RNA using the First-Strand cDNA Synthesis Kit (Thermo Fisher Scientific, USA). The qRT-PCR was performed on CFX96™(Bio-Rad) using the SYBR Green Master Mix (Accurate Biotechnology Co, Ltd, Hunan, AG11701). For SYBR Green qRT-PCR, 4.6 µl of cDNA (10 µg/µl) were mixed with 5 µl of Power SYBR Green PCR Master Mix, 0.2 µl of forward primer (10 µM) and 0.2 µl of reverse primer (10 µM). The cDNA mix was incubated 2 min at 50 °C followed by a denaturation step of 30 s at 95 °C and an amplification step of 40 cycles at 95 °C for 5 s and at 60 °C for 30 s. TRPM2 primers were used as follows: Forward: 5′-GGCAGCCTTGTACTTCAGTGAC-3′ and reverse: 5′-GAGGCAGAACAGGATGAAGTCC-3′.

Phalloidin staining of the actin cytoskeleton

Cells grown on coverslips to ∼50% confluence were treated with different drugs at 37 °C for 2 h in standard buffered saline (SBS; 10 mM HEPES, 130 mM NaCl, 1.2 mM KCl, 8 mM glucose, 1.5 mM $CaCl_2$, 1.2 mM $MgCl_2$, pH 7.4) with or without H_2O_2 or Palmitate (see figure legends). Cells were fixed with 2% paraformaldehyde for 15 min, followed by three washes withphosphate-buffered saline (PBS). Cells were then permeabilised with 0.2% Triton X-100 and 5% goat serum in PBS for 15 min and labelled with Alexa-Fluor-488-conjugated phalloidin (1:1000 in goat serum). Images were collected with an LSM800 confocal microscope using a 63 ×1.4 NA oil objective with an appropriate excitation and emission wavelengths.

Ca^{2+} and Zn^{2+} imaging

Cytosolic Ca^{2+} and Zn^{2+} levels were determined as described previously [24, 25]. Cells were seeded onto 35 mm glass bottomed dishes and grown to approximately 60% confluence. Cells were then incubated with Fluo4-AM or Fluozin3-AM (1 µM) in SBS containing 0.01% pluronic F127 at 37 °C for 2 h and then treated with compounds as desired. Subsequently cells were washed with PBS once followed by imaging with an LSM700 inverted confocal microscope using 63 ×/1.4 NA oil objective. Fluo4-AM and Fluozin3-AM were excited at 488 nm and emission was collected at 510 nm.

(See figure on next page.)

Fig. 1 H_2O_2 activation of TRPM2 channels causes a rise in cytosolic level of Ca^{2+}. **A** PC-3 cells were treated without (CTRL) or with H_2O_2 (100 µM) minus or plus ACA (2.5 µM), Clotrimazole (10 µM) and Econazole (10 µM). The cells were loaded with Fluo4-AM and analyzed by ImageJ; representative confocal images are shown; scale bars = 20 µm. **B** Mean ± SEM of average Ca^{2+} fluorescence per cell (CTRL: 132 cells; H_2O_2: 129 cells; ACA: 143 cells; Clotrimazole: 124 cells; Econazole: 138 cells) from three independent experiments performed as in (**A**); **** indicates $p < 0.0001$; one-way Anova, with post-hoc Tukey test. **C** PC-3 cells transfected with scrambled siRNA or siRNA against TRPM2 were either not treated (CTRL) or treated with H_2O_2 (100 µM) and loaded with Fluo4-AM and analyzed by ImageJ; representative confocal images are shown; scale bars = 20 µm. **D** Mean ± SEM of average Ca^{2+} fluorescence per cell (CTRL: 137 cells; H_2O_2: 128 cells; ACA: 136 cells; Clotrimazole: 129 cells; Econazole: 136 cells) from three independent experiments performed as in (**C**); **** indicates $p < 0.0001$; one-way Anova, with post-hoc Tukey test. **E** PC-3 cells were loaded with Fura-2-AM for 1 h followed with three times washing; cells were then treated as follows: CTRL (SBS alone); H_2O_2 (SBS alone); BAPTA-AM (SBS containing 10 µM BAPTA-AM); EGTA (SBS containing 1.5 mM EGTA) for 1 h at 37 °C and then cytosolic Ca^{2+} were measured by Flexstation Microplate Reader; at 60 s, H_2O_2 was added to H_2O_2 wells and wells containing BAPTA-AM and EGTA pre-treated cells. The fluorescence ratio of 340/380 was recorded. **F** Mean ± SEM of fluorescence amplitude from at least three independent experiments performed as in (**E**). * Indicates $p < 0.05$; **** indicates $p < 0.0001$; one-way Anova with post-hoc Tukey test

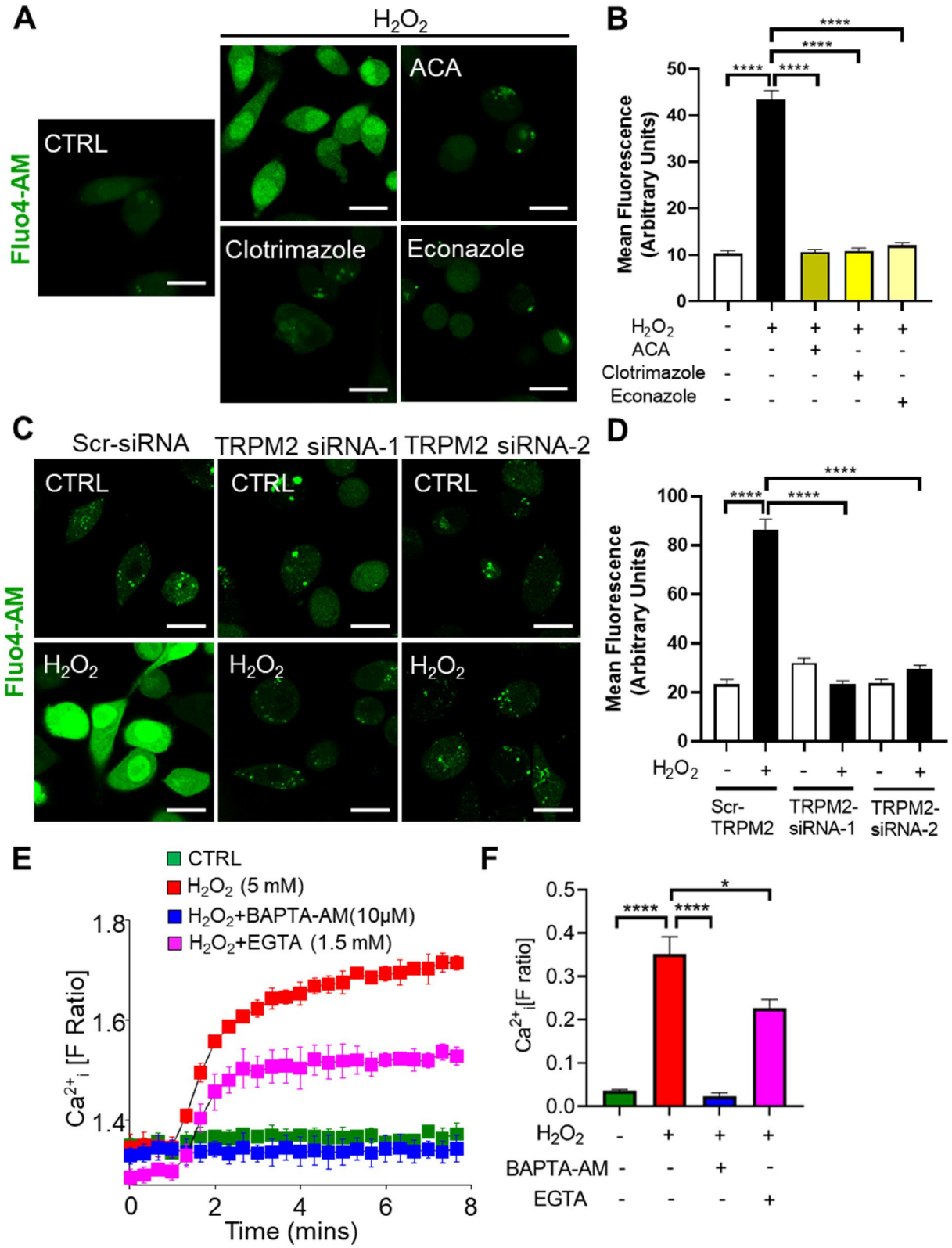

Fig. 1 (See legend on previous page.)

Intracellular Ca^{2+} and Zn^{2+} measurements by Flexstation

Intracellular Ca^{2+} and Zn^{2+} were monitored using Fura-2-AM and FluoZin3-AM respectively and fluorescence was examined using a Molecular Devices Flexstation (Price and Lummis, 2005). Cells were plated at approximately 40,000 cells per well on clear-bottomed 96-well plates (Costar) and grown overnight. Cells were then incubated in Fura-2-AM (2 μM) or FluoZin3-AM made up in SBS (pH 7.4) containing 0.01% Pluronic F-127 for 1 h at 37 °C. After washing twice with SBS, 200 μl SBS were added. Then the Zn^{2+} fluorescence was monitored directly at 530 nm (excitation wavelength of 490 nm) and the data are expressed as change in F. For Ca^{2+} measurement, the appropriate reagents were prepared and plated onto a round-bottomed 96-well plate. Both plates were loaded onto Flexstation® 3 Multi-Mode Microplate Reader (Molecular Devices, California, USA). Fluorescence was measured for a total 7 min at 10 s intervals using excitation wavelengths of 340 and 380 nm and emission wavelength of 510 nm. At taking control measurements for ~65 s, 50 μl of the reagents made up at five-fold the required final concentration was added to wells. The ratio of fluorescence intensities following excitation at 340 and 380 nm was calculated for each measurement point. For statistical comparisons, the mean of the ratios in the last time-point minus baseline was calculated for each treatment and the statistical differences were compared using one-way Anova.

Cell migration assay

Directional cell migration was examined by performing an agarose spot assay as described previously [25, 26]. Briefly, 90 μL of 0.5% molten low-melting-point agarose (Invitrogen) maintained at 40 °C was pipetted into 1.5-ml Eppendorf tubes containing 10 μl PBS with or without desired substances. A total of 10 μl of agarose was then spotted (four spots per plate) onto six-well plates and allowed to cool for 8 min at 4 °C. Cells were then plated to ~60% confluence in a complete medium containing 10% FCS and allowed to adhere for 4 h before replacing with fresh medium containing 0.1% FCS. After 16 h at 37 °C, images were collected using an EVOS®FL microscope fitted with a 10 ×objective (Life Technologies). For each spot, cells that penetrated underneath the agarose spot were recorded as migrating cells.

DCF-DA staining

Cytosolic ROS production was measured by using cell-permeant 2', 7'di-chlorodihydro fluorescein diacetate (H2DCF-DA) (Biotium). Briefly, cells were treated with various agents for the desired length of time and then incubated with HBSS containing 10 μM H2DCF-DA for 30 min at 37°C/5% CO_2. The cells were then washed three times with HBSS prior to loading onto the inverted confocal microscopy using 40 ×/1.4 NA oil objective for imaging (excitation, 488 nm; emission, 515–540 nm).

Quantification of filopodia and Lamellipodia

Quantification of filopodia was carried out as described previously [27]. Phalloidin-positive spike-like structures at cell periphery were counted as filopodia. A filopodium with branches was counted as one. Filopodia from five cells of an individual experiment were counted. Lamellipodia were identified as a convex stretch of perpendicular actin stain at the peripheral edge of the cell as visualized by the Alexa-Fluor 488-labeled phalloidin stain [28].

Data analysis and presentation

All experiments were performed at least three times (n) and the values presented as mean ± S.E.M. Representative confocal images are presented. Fluorescence of cells was quantified using Image J (NIH). Statistical significance was determined using the Student's t-test or one-way ANOVA, followed by Tukey's post hoc test. Probability (p) values are indicated with *, ** and ***, which correspond to values of 0.05, 0.01 and 0.001, respectively.

Results

H_2O_2 activation of TRPM2 channels causes a rise in cytosolic level of Ca^{2+}

In most cell types, TRPM2 channels are expressed at the plasma membrane of the cell where they promote Ca^{2+} entry from the extracellular source upon activation by H_2O_2 [25, 29]. In some cell types, however, TRPM2 channels are reported to be located in the lysosomal

(See figure on next page.)

Fig. 2 TRPM2 channels mediate H_2O_2 induced cytosolic Zn^{2+} increase in PC-3 cells. **A** PC-3 cells were treated without (CTRL) or with H_2O_2 (100 μM) minus or plus ACA (2.5 μM), Clotrimazole (10 μM) and Econazole (10 μM). The cells were loaded with Fluozin-3-AM and analyzed by ImageJ; representative confocal images are shown; scale bars = 20 μm. **B** Mean ± SEM of average Zn^{2+} fluorescence per cell (CTRL: 144 cells; H_2O_2: 123 cells; ACA: 136 cells; Clotrimazole: 135 cells; Econazole: 133 cells) from three independent experiments performed as in (A); **** indicates $p < 0.0001$; one-way Anova, with post-hoc Tukey test. **C** PC-3 cells transfected with scrambled siRNA or siRNA against TRPM2 were either not treated (CTRL) or treated with H_2O_2 (100 μM) and loaded with Fluozin-3-AM and analyzed by ImageJ; representative confocal images are shown; scale bars = 20 μm. **D** Mean ± SEM of average Zn^{2+} fluorescence per cell (CTRL: 139 cells; H_2O_2: 127 cells; ACA: 138 cells; Clotrimazole: 133 cells; Econazole: 135 cells) from three independent experiments performed as in (**C**); **** indicates $p < 0.0001$; one-way Anova, with post-hoc Tukey test. **E** Staining of PC-3 cells with FluoZin3-AM (green) and indicators of organelles (red); representative confocal images are shown; scale bars = 20 μm

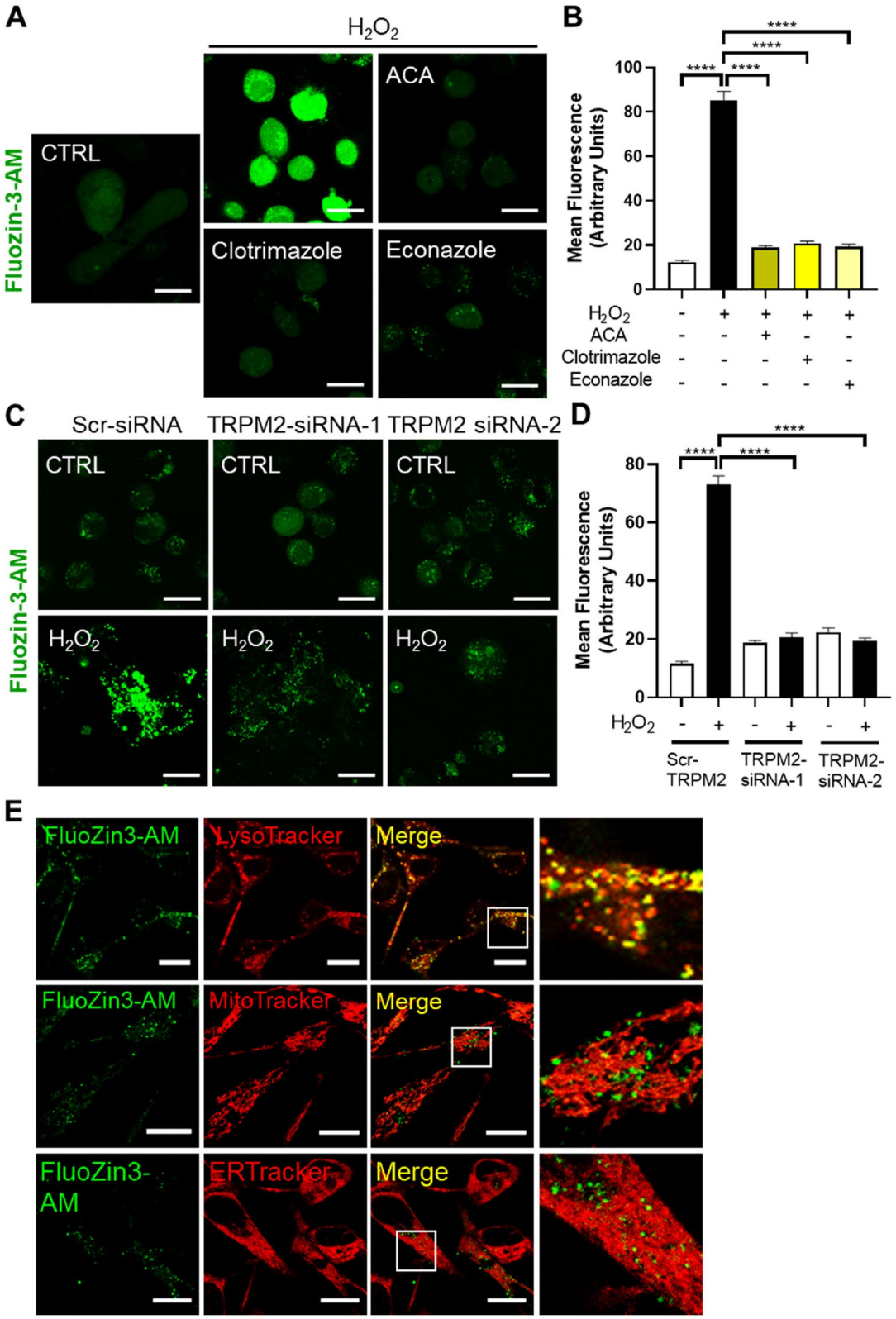

Fig. 2 (See legend on previous page.)

membranes to mediate lysosomal Ca^{2+} release [30, 31]. Therefore, to examine H_2O_2-induced Ca^{2+} changes in prostate cancer cells, the Fluo4-AM Ca^{2+} reporter was introduced into the PC-3 cells and DU145 cells. H_2O_2 caused a marked rise in intracellular fluorescence as detected by confocal microscopy in both PC-3 cells and DU145 cells (Fig. 1A, B and Supplementary Figure 2A-B). Inhibition of TRPM2 channels with N- (p-amylcinnamoyl) anthranilic acid (ACA) [32], clotrimazole and econazole [33], three previously reported TRPM2 inhibitors, suppressed the H_2O_2 induced intracellular fluorescence in both PC-3 cells and DU145 cells. Further siRNAs (siRNA-1 and siRNA-2) targeted to TRPM2 channels (Supplementary Figure 1), but not the scrambled control siRNA, suppressed H_2O_2 induced Ca^{2+} increase (Fig. 1C, D), indicating a role for TRPM2 channels in the Ca^{2+} increase.

To assess whether this cytosolic Ca^{2+} rise involves both Ca^{2+} entry and release, BAPTA-AM, a cell membrane-permeable Ca^{2+} chelator and EGTA were used to chelate intracellular Ca^{2+} and extracellular Ca^{2+} respectively. In consistent with the confocal data, H_2O_2 induced robust elevation of intracellular Ca^{2+} concentration. Chelation of extracellular Ca^{2+} with EGTA, partially reduced the Ca^{2+} signal. BAPTA-AM, on the other hand, completely abolished the Ca^{2+} signal (Fig. 1E, F).

Collectively, these results suggest that H_2O_2 induces both Ca^{2+} entry and release in prostate cancer cells, which is largely mediated by TRPM2 channels.

TRPM2 channels mediate H_2O_2-induced cytosolic increase of Zn^{2+}

In addition to raising cytosolic Ca^{2+}, H_2O_2 activation of TRPM2 channels can also increase cytosolic Zn^{2+} in INS-1 cells [24] and TRPM2 transfected HEK-293 cells [34]. As Zn^{2+} even at sub-millimolar concentrations completely inhibits TRPM2 channels, it is impossible to record Zn^{2+}-carrying currents using electrophysiology [35]. Therefore, we used FluoZin-3-AM, a Zn^{2+}-specific fluorophore, to examine whether H_2O_2 causes Zn^{2+} rise in prostate cancer cells. We demonstrated that H_2O_2 induced a remarkable increase in FluoZin-3 fluorescence in both PC-3 cells (Fig. 2A, B) and DU145 cells (Supplementary Fig. 2C-D). Chemical or siRNA inhibition of TRPM2 channels abolished the rise in the cytosolic levels of Zn^{2+}(Fig. 2A-D and Supplementary Figure 2C-D). These results indicate TRPM2 dependent rise in cytosolic $[Zn^{2+}]$.

Since H_2O_2 induced Zn^{2+} release is from an intracellular source, the location of free Zn^{2+} was examined. Co-staining of cells with FluoZin-3-AM (green) and indicators of intracellular organelles (red) showed significant colocalization of Zn^{2+} stain with LysoTracker (Fig. 2E), indicating that the source of the Zn^{2+} is likely lysosomes.

Taken together, the results show that H_2O_2-mediated activation of TRPM2 channels increases the cytosolic levels of not only Ca^{2+} but also Zn^{2+}.

Zn^{2+}, rather than Ca^{2+}, mediates H_2O_2-induced actin remodelling

We have demonstrated in our previous study that TRPM2 channels mediate H_2O_2 induced actin remodelling in PC-3 cells[25], moreover, our above data has shown that TRPM2 channels mediate rise in both Ca^{2+} and Zn^{2+}. Therefore, to get an insight into the individual role of Ca^{2+} and Zn^{2+} in H_2O_2 induced actin remodelling of prostate cancer cells, we used BAPTA-AM and TPEN, a Zn^{2+} selective chelator, to chelate Ca^{2+} and Zn^{2+} respectively. Alexa-Fluor-488-conjugated phalloidin was used to monitor actin cytoskeleton change. Chelation of Zn^{2+} indeed showed a striking effect on the actin cytoskeleton: it prevented H_2O_2 induced filopodia formation and loss of stress fibres. By contrast, chelation of Ca^{2+} had less effect on filopodia formation in both PC-3 cells (Fig. 3A,

(See figure on next page.)

Fig. 3 Zn^{2+}, rather than Ca^{2+}, mediates H_2O_2 induced actin remodelling and cell migration. **A** Cells were either not treated (CTRL) or treated with H_2O_2 (100 μM) plus or minus BAPTA-AM (10 μM) and TPEN (5 μM) and then stained for F-actin. Representative images are shown; scale bars = 20 μm. **B** Mean ± SEM of filopodia number (5 cells) from three independent experiments performed as in (**A**); *** indicates $p < 0.001$; NS, not significant; one-way Anova with post-hoc Tukey test. **C** PC-3 cells were loaded with Fura-2-AM for 1 h followed with three times washing; cells were then treated as follows: CTRL (SBS alone); A23187(SBS alone); BAPTA-AM (SBS containing 10 μM BAPTA-AM) for 1 h at 37 °C and then cytosolic Ca^{2+} were measured by Flexstation Microplate Reader; at 60 s, A23187 was added to A23187 wells and wells containing BAPTA-AM pre-treated cells. The fluorescence ratio of 340/380 was recorded. **D** Mean ± SEM of fluorescence amplitude from at least three independent experiments performed as in (**C**). **** indicates $p < 0.0001$; one-way Anova with post-hoc Tukey test. **E** Cells were loaded with FluoZin3-AM for 1 h with three times washing; cells were then treated without (CTRL) or with ZnPTO (3 μM) plus or minus TPEN (5 μM) for 2 h 37 °C and cytosolic Zn^{2+} were measured by Flexstation Microplate Reader. The fluorescence was recorded. **F** Mean ± SEM of fluorescence from at least three independent experiments performed as in (**E**). ** indicates $p < 0.01$; *** indicates $p < 0.001$; one-way Anova with post-hoc Tukey test. **G** F-actin was stained following buffer (CTRL), A23187 (3 μM) minus or plus BAPTA-AM (10 μM) and ZnPTO (3 μM) minus or plus TPEN (5 μM) treatments. Representative images are shown; scale bars = 20 μm. **H** Mean ± SEM of filopodia number (5 cells) from three independent experiments performed as in (**G**); *** indicates $p < 0.001$; NS, not significant

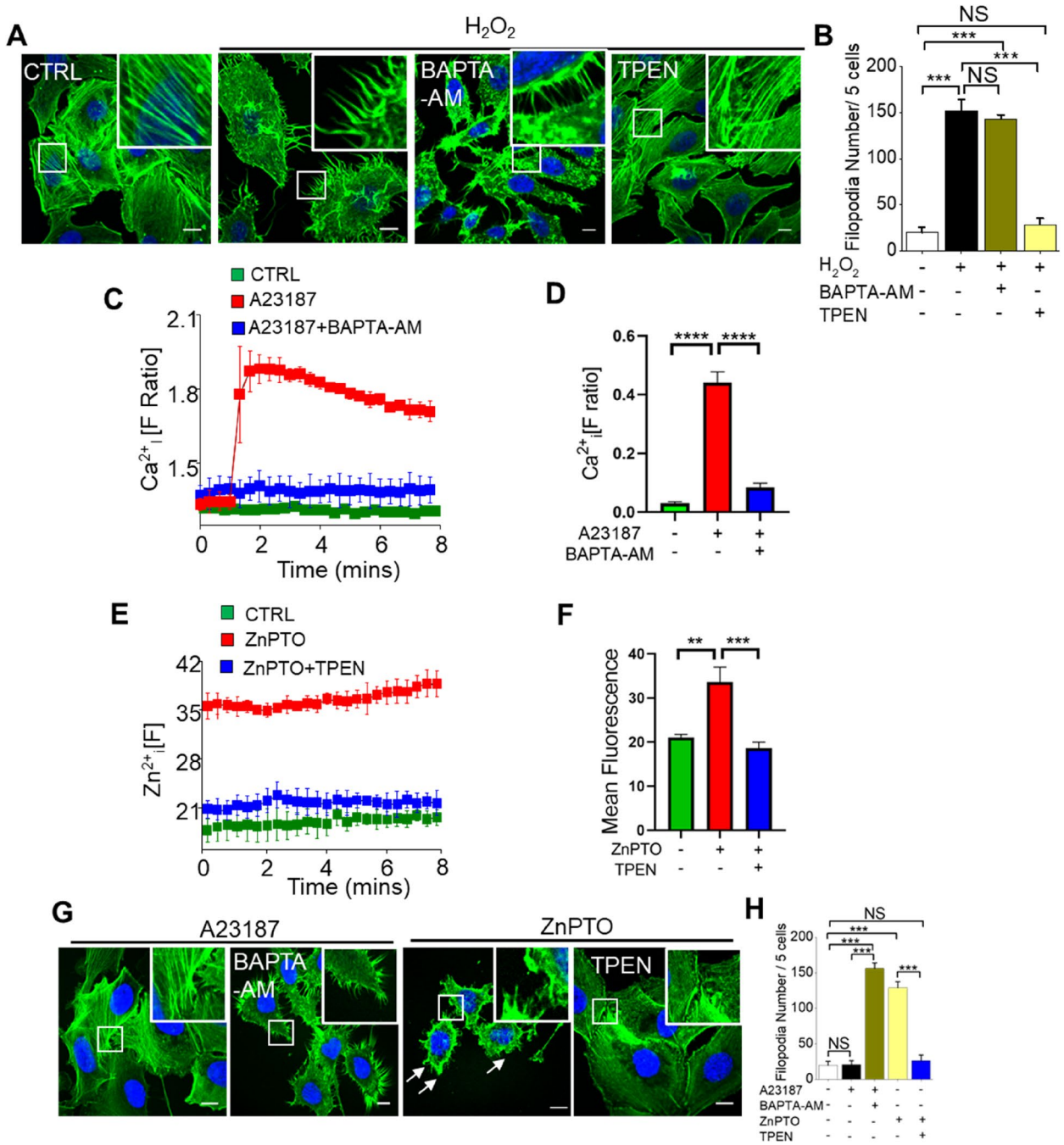

Fig. 3 (See legend on previous page.)

B) and DU145 cells (Supplementary Figure 3A-B). This is consistent with our previous findings in HeLa cells.

To directly examine the individual effect of Ca^{2+} and Zn^{2+} on actin cytoskeleton, we applied the Ca^{2+} and Zn^{2+} ionophores in absence of H_2O_2. Prior to their use, we verified the efficacy of the probes: A23187 caused an increase in cytosolic Ca^{2+} which was antagonized by BAPTA-AM (Fig. 3C, D); and zinc pyrithione (Zn-PTO) caused a rise in cytosolic Zn^{2+} that was blocked by TPEN (Fig. 3E, F).

Besides, we found A23187 had no obvious effect on actin cytoskeleton, while, co-incubation with BAPTA-AM disrupted stress fibres and induced filopodia formation (Fig. 3G, H). Zn-PTO induced loss of stress fibres and formation of apparent filopodia, and TPEN, reversed these effects both in PC-3 cells (Fig. 3G, H) and DU145

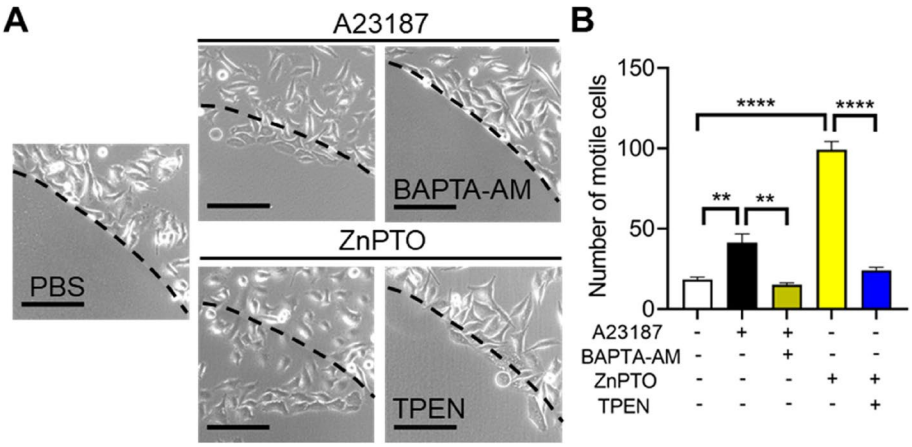

Fig. 4 Zn^{2+} plays a priority role in promoting cell migration. **A** Agarose spots containing PBS, A23187 minus or plus BAPTA-AM, or ZnPTO with or without TPEN were loaded into 6-well plates and then cells were plated around the agarose spots. **B** Mean ± SEM of number of motile cells per spot; data were from three independent experiments performed as in (**A**). In all cases, representative images of a section of the spot and surrounding area are shown, broken line indicates agarose boundary; ** indicates $p < 0.01$; **** indicates $p < 0.0001$; one-way Anova with post-hoc Tukey test. Scale bars: 200 µm

cells (Supplementary Figure 3C-D). Surprisingly, we noticed that Zn-PTO induced fan-like lamellipodia formation (Fig. 3G, H, indicated by white arrows). Lamellipodia are brush-like protrusions generally formed at the leading edge of migrating cells [5], therefore, Zn^{2+} might have effect on cell migration by regulating filopodia and lamellipodia formation.

Collectively, these results revealed that Zn^{2+}, rather than Ca^{2+}, regulates H_2O_2-induced actin remodelling.

Zn^{2+} plays a priority role in promoting cell migration

We have previously demonstrated that TRPM2 channels mediate H_2O_2-induced directional cell migration in PC-3 cells [25]. As H_2O_2 activation of TRPM2 channels mediate both Ca^{2+} and Zn^{2+} rise, next, we determined the individual effect of Ca^{2+} and Zn^{2+} on cell migration in the absence of H_2O_2. We used an agarose spot cell migration assay [25, 26] where the test compounds were included in the agarose spot and the migration of surrounding cells to the spots was examined. We found inclusion of A23187 in the agarose spot modestly promoted cell migration; there was little migration in the PBS control. BAPTA-AM prevented A23187-induced cell migration (Fig. 4). Zn-PTO, on the other hand, strongly promoted cell migration that was prevented by TPEN (Fig. 4).

These results suggest that Zn^{2+} plays a priority role in promoting PC-3 cell migration.

Palmitate-induced ROS activates TRPM2 to induce actin remodelling

Above data have shown that H_2O_2 (a type of ROS) induces actin remodelling in prostate cancer cells, we next asked whether palmitate, a saturated fatty acid previously to be demonstrated to elevate ROS production [36, 37], produces effect similar to H_2O_2. Since palmitate can produce ROS and its toxicity can vary depending on the cell type [23, 38], we first screened PC-3 for its sensitivity to palmitate (data not shown) and chose a time (< 8 h) and a concentration (500 µM) that is not cytotoxic under the experimental conditions used.

To address this question, we firstly fluorescently stained the actin cytoskeleton and the results showed that

(See figure on next page.)

Fig. 5 TRPM2 channels mediate Palmitate-induced actin remodelling. **A** PC-3 cells were either not treated (CTRL) or treated with palmitate (500 µM) plus or minus ACA (2.5 µM), Clotrimazole (10 µM) and Econazole (10 µM) and then stained for F-actin. Representative images are shown; scale bars = 20 µm. **B** Mean ± SEM of Lamellipodia extent (5 cells) from three independent experiments performed as in (**A**); **** indicates $p <$ 0.0001; one-way Anova with post-hoc Tukey test. **C** PC-3 cells transfected with scrambled siRNA or siRNA against TRPM2 were either not treated (CTRL) or treated with palmitate (500 µM) and then stained for F-actin. Representative images are shown; scale bars = 20 µm. **D** Mean ± SEM of Lamellipodia extent (5 cells) from three independent experiments performed as in **C**; **** indicates $p < 0.0001$; one-way Anova with post-hoc Tukey test. **E** Live cell fluorescent images of PC-3 cells exposed to medium alone (CTRL), medium containing palmitate (500 µM) with or without NAC (10 mM). Cells were stained for cytosolic ROS (H2DCF-DA). Scale bars: 10 µm. **F** Mean ± SEM of data from (**E**) expressed as mean fluorescence per cell from the three independent experiments following the indicated treatments; **** indicates $p < 0.0001$; one-way Anova with post-hoc Tukey test

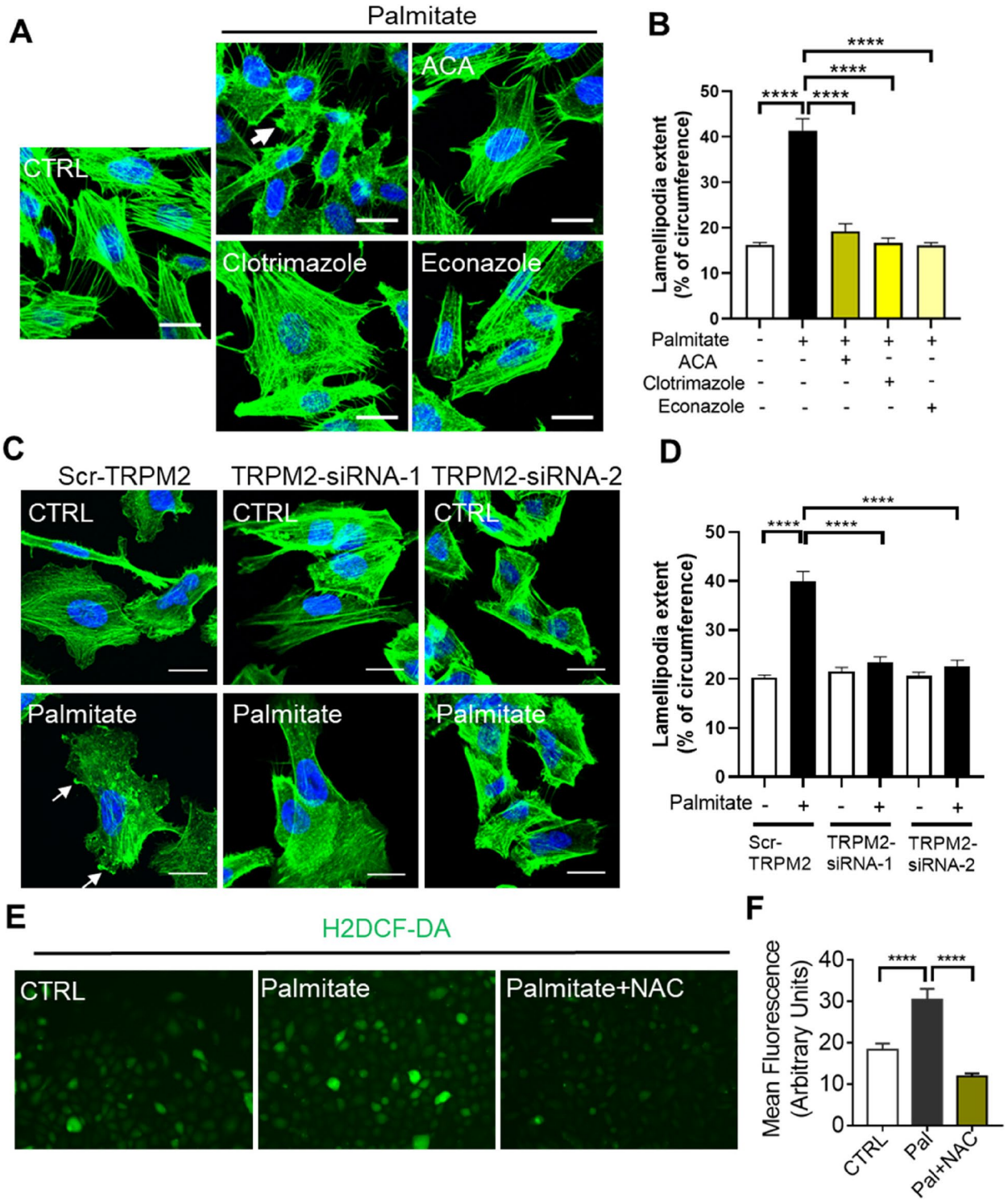

Fig. 5 (See legend on previous page.)

palmitate induced numerous lamellipodia with distinct filopodia in both PC-3 cells (Fig. 5A, B) and DU145 cells (Supplementary Figure 4A-B). This finding is interesting as H_2O_2 induces apparent filopodia with less lamellipodia (Fig. 3A-B). Besides, we found ACA, clotrimazole and econazole, suppressed palmitate induced filopodia and lamellipodia formation (Fig. 5A, B and Supplementary Figure 4A-B). Knock-down of TRPM2 channels with

siRNA abolished the formation of filopodia and lamellipodia (Fig. 5C, D), indicating the role of TRPM2 channels in actin remodeling induced by palmitate.

Since NAC attenuated the Palmitate induced actin remodelling (data not shown), we predicted that palmitate might induce ROS production to induce changes in actin cytoskeleton. We stained cells with H2DCF-DA, a ROS detection reagent. Consistent with the expectation, we found cells under palmitate treatment displayed significantly greater levels of staining which was fully eliminated by NAC (Fig. 5E, F).

Taken together, these results suggest that palmitate induced changes in actin cytoskeleton are mediated by ROS and TRPM2 channels.

TRPM2-mediated Zn^{2+}, rather than Ca^{2+}, mediates Palmitate-induced actin remodelling

Since Palmitate induces generation of ROS, by which TRPM2 is activated to conduct both Ca^{2+} [21, 39] and Zn^{2+} [24], we next examined the effect of Palmitate on cytosolic Ca^{2+} and Zn^{2+} dynamics in PC-3 cells. Palmitate caused a marked rise in intracellular cytosolic Ca^{2+} and Zn^{2+} in both PC-3 cells (Fig. 6) and DU145 cells (Supplementary Figure 5). Chemical or siRNA inhibition of TRPM2 channels suppressed the fluorescence signal (Fig. 6 and Supplementary Figure 5). These results suggest that TRPM2 channels mediate palmitate induced cytosolic Ca^{2+} and Zn^{2+} increase.

To investigate the effect of Ca^{2+} and Zn^{2+} dynamics on actin cytoskeleton, we stained the actin cytoskeleton in PC-3 cells. The results showed that palmitate markedly disrupted the stress fibers and promoted lamellipodia formation. Chelation of Ca^{2+} by BAPTA-AM showed little effect on filopodia and lamellipodia formation while chelation of Zn^{2+} by TPEN reversed Palmitate-induced loss of stress fibers and lamellipodia formation (Fig. 7).

These data suggest that TRPM2 channels mediate Palmitate-induced actin cytoskeleton rearrangement by raising cytosolic Zn^{2+}, rather than cytosolic Ca^{2+}.

TRPM2 channels mediate Palmitate-induced cell migration

Given that filopodia and lamellipodia are formed at the leading edge of migrating cells, we further investigated whether the formation of filopodia and lamellipodia induced by palmitate will increase PC-3 cell migration. We performed the agarose spot assay. Consistent with the expectation, inclusion of Palmitate in the agarose spot increased migration of cells into the spot. ACA inhibited Palmitate-induced cell migration (Fig. 8A, B). siRNAs targeted against TRPM2 channels, but not scrambled siRNA, prevented Palmitate-induced cell migration (Fig. 8C, D). To further confirm the role of palmitate and TRPM2 channels in cell migration, a Boyden's chamber assay was performed. We found cell migration was enhanced by palmitate, which was inhibited by ACA, clotrimazole and econazole (data not shown).

Collectively, these data suggest a role for TRPM2 channels in Palmitate-induced cell migration.

Discussion

The effects of ROS on cytoskeleton remodeling have been described in numerous studies. For example, NADPH oxidase (NOX)-mediated ROS generation has been shown to be necessary for the formation of invadopodium in cancer cells [40]. Here, we revealed artificial ROS (from H_2O_2) or ROS produced upon palmitate treatment promoted migration of PC-3 cells by regulating filopodia and lamellipodia formation. Moreover, we found TRPM2 channels serves as a downstream effector of these types of ROS. By permeating Zn^{2+}, TRPM2 channels regulate

(See figure on next page.)

Fig. 6 Palmitate-induced rise of cytosolic Ca^{2+} and Zn^{2+} is dependent on TRPM2 channels. **A** PC-3 cells were treated without (CTRL) or with palmitate (500 μM) minus or plus ACA (2.5 μM), Clotrimazole (10 μM) and Econazole (10 μM). The cells were loaded with Fluo4-AM and analyzed by ImageJ; representative confocal images are shown; scale bars = 20 μm. **B** Mean ± SEM of average Ca^{2+} fluorescence per cell (CTRL: 129 cells; H_2O_2: 120 cells; ACA: 132 cells; Clotrimazole: 134 cells; Econazole: 128 cells) from three independent experiments performed as in (**A**); **** indicates $p < 0.0001$; one-way Anova, with post-hoc Tukey test. **C** PC-3 cells transfected with scrambled siRNA or siRNA against TRPM2 were either not treated (CTRL) or treated with palmitate (500 μM) and loaded with Fluo4-AM and analyzed by ImageJ; representative confocal images are shown; scale bars = 20 μm. **D** Mean ± SEM of average Ca^{2+} fluorescence per cell (CTRL: 129 cells; H_2O_2: 118 cells; ACA: 126 cells; Clotrimazole: 128 cells; Econazole: 131 cells) from three independent experiments performed as in (**C**); **** indicates $p < 0.0001$; one-way Anova, with post-hoc Tukey test. **E** PC-3 cells were treated without (CTRL) or with palmitate (500 μM) minus or plus ACA (2.5 μM), Clotrimazole (10 μM) and Econazole (10 μM). The cells were loaded with Fluozin-3-AM and analyzed by ImageJ; representative confocal images are shown; scale bars = 20 μm. **F** Mean ± SEM of average Zn^{2+} fluorescence per cell (CTRL: 129 cells; H_2O_2: 118 cells; ACA: 126 cells; Clotrimazole: 128 cells; Econazole: 131 cells) from three independent experiments performed as in (**E**); **** indicates $p < 0.0001$; one-way Anova, with post-hoc Tukey test. **G** cells transfected with scrambled siRNA or siRNA against TRPM2 were either not treated (CTRL) or treated with palmitate (500 μM) and loaded with Fluozin-3-AM and analyzed by ImageJ; representative confocal images are shown; scale bars = 20 μm. **H** Mean ± SEM of average Zn^{2+} fluorescence per cell (CTRL: 129 cells; H_2O_2: 118 cells; ACA: 126 cells; Clotrimazole: 128 cells; Econazole: 131 cells) from three independent experiments performed as in (**G**); **** indicates $p < 0.0001$; one-way Anova, with post-hoc Tukey test

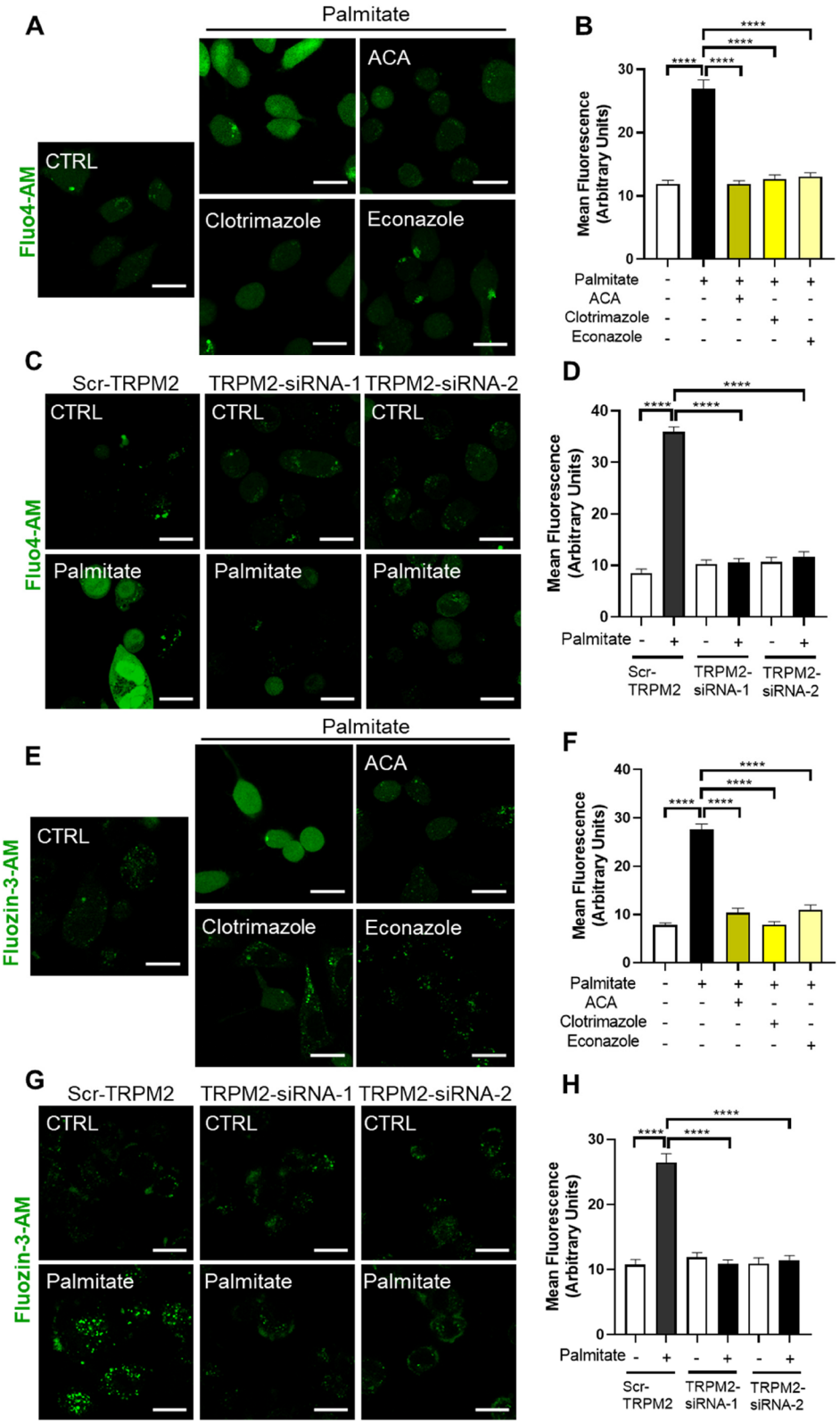

Fig. 6 (See legend on previous page.)

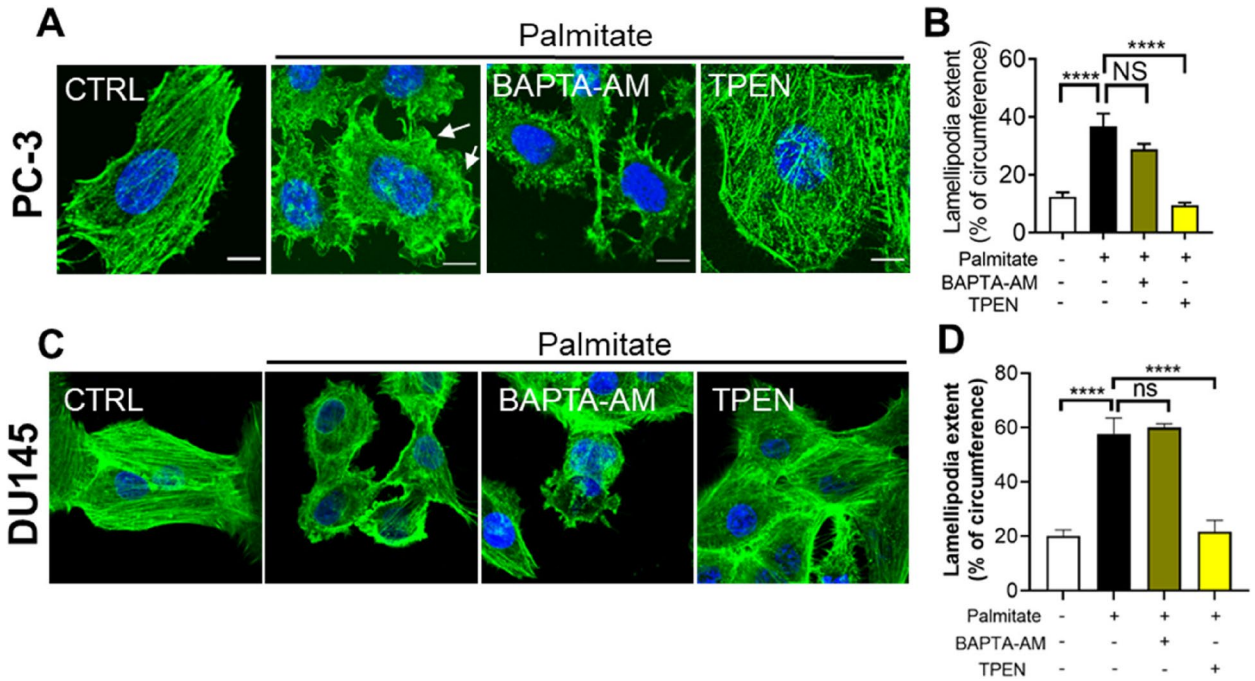

Fig. 7 Zn^{2+}, rather than Ca^{2+}, mediates H_2O_2-induced actin remodelling in PC-3 cells and DU145 cells. **A** PC-3 cells were either not treated (CTRL) or treated with Palmitate (500 μM) plus or minus BAPTA-AM (10 μM) and TPEN (5 μM) and then stained for F-actin. Representative images are shown; scale bars = 20 μm. **B** Mean ± SEM of Lamellipodia extent (5 cells) from three independent experiments performed as in (**A**). **** indicates $p < 0.0001$; NS, not significant; one-way Anova with post-hoc Tukey test. **C** DU145 cells were either not treated (CTRL) or treated with palmitate (500 μM) plus or minus BAPTA-AM (10 μM) and TPEN (5 μM) and then stained for F-actin. Representative images are shown; scale bars = 20 μm. **D** Mean ± SEM of Lamellipodia extent (5 cells) from three independent experiments performed as in (**C**); **** indicates $p < 0.0001$; ns, on not significant; one-way Anova with post-hoc Tukey test

actin remodeling and migration of prostate cancer cells induced by H_2O_2 and palmitate. As elevated free fatty acid level is a hallmark for type 2 diabetes (T2D), these results provide evidences for the role of ROS as a factor linking cancer and diabetes and TRPM2 may act as a molecular link downstream of ROS.

The regulation of actin filaments by Ca^{2+} has been extensively studied. In neurons, low levels of local Ca^{2+} transients facilitate filopodia outgrowth while high levels inhibit the formation of filopodia [41]. In prostate cancer cells, inhibition of Ca^{2+}/calmodulin dependent protein kinase (CaMKII) increases the frequency and length of filopodia, indirectly supporting the inhibitory role of Ca^{2+} on filopodia formation [42]. Consistent with these reports, our finding that chelation of Ca^{2+} by BAPTA-AM produced more filopodia (Fig. 3A, B and G, H) suggest the inhibitory effect of Ca^{2+} on filopodia formation. As whether this Ca^{2+} responsible for filopodia prevention requires to be constrained in subcellular compartment or should beyond the threshold remains to be investigated.

In our previous study, we have reported the effect of Zn^{2+} on filopodia formation in Hela cells. However, the link between Zn^{2+} and actin cytoskeleton in cancer cells remains largely unknown. There are some indirect evidences. For example, Zn^{2+} can induce ERK signaling pathway [43], which has been demonstrated to reinforce the cellular protrusions during cell migration [44]. Here, consistent with our previous findings [25], we found H_2O_2 caused a marked rise in both cytosolic [Ca^{2+}] (Fig. 1) and [Zn^{2+}] (Fig. 2A, D) which is dependent on the activation of TRPM2 channels. Besides, depletion of Zn^{2+} alone was found to be sufficient to prevent H_2O_2-induced actin rearrangement (Fig. 3A, B) and elevation of cytosolic [Zn^{2+}] with Zn-PTO produced effects that were almost identical to those caused by H_2O_2 (Fig. 3A, G). However, we were unable to explore the underlying mechanism of Zn^{2+} in H_2O_2-induced actin remodeling and further studies are required.

TRPM2 is a non-selective, Ca^{2+}-permeable cation channel which is highly sensitive to ROS [21]. A previous study has reported the increased TRPM2 expression levels in human prostate cancer samples were correlated with higher grade levels [45]. TRPM2 contribute to prostate cancer growth and progression by negatively regulating autophagy-related and apoptosis-related genes [45] and promoting cell proliferation [46]. Furthermore, TRPM2 channels can affect cancer cell migration. For example, TRPM2 downregulation markedly inhibits

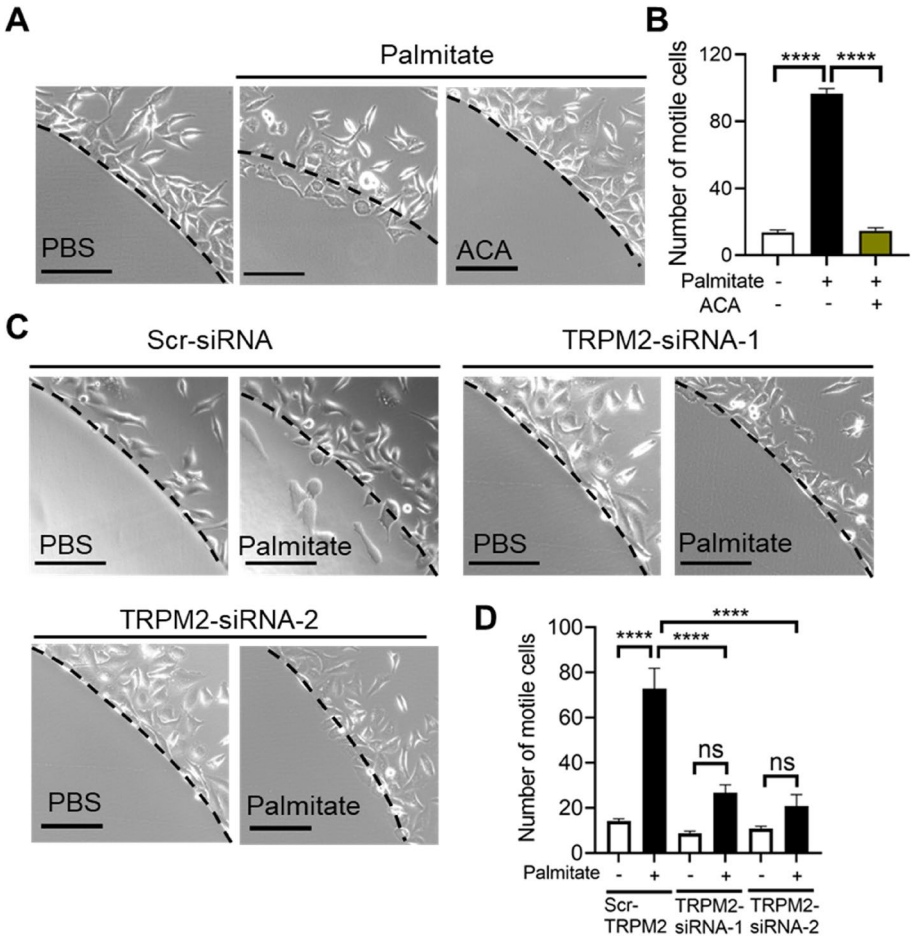

Fig. 8 Palmitate-induced cell migration is TRPM2 dependent. **A** Agarose spots containing PBS, 500 µM palmitate or palmitate plus 2-APB were plated onto 6-well plates and then cells were plated around the agarose spots followed by incubation for 16 h at 37ºC. **C** PC-3 cells transfected with scrambled siRNA or siRNA against TRPM2 were plated onto a 6-well plate containing PBS (CTRL) or 500 µM palmitate-containing agarose spots. **B** and **D** Mean ± SEM of number of motile cells per spot; data were from three independent experiments performed as in (**A**) and (**C**) respectively. In all cases, representative images of a section of the spot and surrounding area are shown, broken line indicates agarose boundary; **** indicates $p < 0.0001$; ns, not significant; one-way Anova with post-hoc Tukey test. Scale bars: 200 µm

gastric cancer cell migration and invasion abilities [47]. Barbara et al. demonstrated that high expression of TRPM2 in neuroblastoma cells promote migration and invasion through regulating integrin activation [48]. Here, we found TRPM2 channels mediate both Ca^{2+} and Zn^{2+} elevation in response to H_2O_2 (Figs. 1 and 2). It is likely that H_2O_2 activation of TRPM2 channels regulate dynamics of actin cytoskeleton by affecting the homeostasis of Ca^{2+} and Zn^{2+}.

Ca^{2+} signaling is important for cell migration and the effects on cell migration are dependent on microenvironments and physiology of different cells [49, 50]. For example, in breast cancer cells, Ca^{2+} elevation increases turnover of focal adhesions, thereby inducing cell migration [51]. While in DU145 and PC-3 cells, transient receptor potential melastatin 8 (TRPM8)-mediated Ca^{2+} inhibits cell migration by impairing cytoskeletal dynamics and focal adhesion formation [52]. Besides, some studies demonstrated that Ca^{2+} gradient is more important for cell migration compared to global Ca^{2+} increase [19, 53]. Zn^{2+} also plays an important role in cell migration [54, 55]. Our data showed that elevation of cytosolic Zn^{2+} induced significant migration in PC-3 cells in agarose-spot cell migration assay while chelation of Zn^{2+} prevented PC-3 cell migration (Fig. 4). Interestingly, elevation of cytosolic Ca^{2+} promoted cell migration although the effect is less compared to that of Zn-PTO (Fig. 4). These findings are comprehensive as above results have demonstrated that Zn^{2+} mediates both filopodia and lamellipodia formation that contributes to cell migration while Ca^{2+} showed little effect on actin cytoskeleton. Therefore, Ca^{2+} might regulate directional cell migration by adopting other machinery [56], rather than actin cytoskeleton. Ca^{2+} might activate TRPM4

channels to induce the expression of epithelial– mesenchymal transition (EMT) markers, thereby enhancing the migratory ability of prostate cancer cells [56]. In future work, the molecular basis for how the Ca^{2+} and Zn^{2+} signal regulates cell migration in a spatio-temporal manner, remains to be investigated.

It is known for a long time that many cancers are dependent on glycolysis for energy [57], therefore cancers might favor the environment with high glucose, such as hyperglycemia in T2D. Consistent with this, a study reported that high glucose promotes migration of gastric cancer cells [58]. Apart from hyperglycemia, in T2D, free fatty acids released from adipose tissues may also play a role in cancer progression [59]. the saturated fatty acid, palmitate, has been reported to induce cancer cell migration [60]. Our finding that palmitate can induce actin remodeling and cell migration is consistent with these findings. Furthermore, we found palmitate presence enhances formation of both filopodia and lamellipodia in PC-3 and DU145 cells, and this effect is dependent on TRPM2 channels (Fig. 5A-D and Supplementary Figure 4). The effect of palmitate on cytosleletal changes has been reported in mouse podocytes [61]. The authors revealed that palmitate induced both mitochondrial and cytosolic ROS to affect actin cytoskeleton. Our study provides evidence that cytosolic ROS production upon palmitate treatment could be responsible for actin cytoskeleton rearrangement (Fig. 5E, F). Whether palmitate simultaneously promotes mitochondrial ROS production in prostate cancer cells will be investigated in future. Moreover, we found palmitate induced TRPM2-dependent elevation of cytosolic Ca^{2+} and Zn^{2+} (Fig. 6). Besides, palmitate-induced formation of filopodia and lamellipodia was reversed by chelation of Zn^{2+}, rather than Ca^{2+} (Fig. 7). Meanwhile, the inhibition of cell migration by ACA and TRPM2 siRNAs (Fig. 8) suggests that alterations in the cytoskeleton via TRPM2 activation may actively participate in the cell migration induced by palmitate. These findings confirm the role of TRPM2 channels as a potential molecular linker between prostate cancer and T2D.

Conclusion

We report that TPPM2 channels and TRPM2-mediated Zn^{2+} play an essential role in ROS-induced actin remodeling and cell migration of PC-3 cells. The ROS is either from artificial H_2O_2 treatment or endogenous stress induction, such as palmitate. Therefore, prevention of TRPM2 channels and chelation of free form of Zn^{2+} might provide two potential therapeutic opportunities for prevention of metastatic progression of cancer. Further studies, including the identification of molecular targets of Zn^{2+}, are required for a meaningful appreciation of Zn^{2+} in actin cytoskeleton and cancer cell migration.

Abbreviations

ROS	Reactive oxygen species
TRPM2	Transient receptor potential melastatin 2
EGF	Epidermal Growth Factor
PMCA	Plasma membrane Ca^{2+} ATPase
ACA	N- (p-amylcinnamoyl) anthranilic acid
Zn-PTO	Zinc pyrithione
NOX	NADPH oxidase
CaMKII	Ca^{2+}/calmodulin dependent protein kinase
T2D	Type 2 diabetes
TRPM8	Transient receptor potential melastatin 8
EMT	Epithelial– mesenchymal transition

Supplementary Information

The online version contains supplementary material available at https://doi.org/10.1186/s12885-025-14333-3.

Supplementary Material 1: Figure S1. Protein and mRNA expression of TRPM2 channels in PC-3 cells and suppression by siRNA. (A) Western blot analysis of TRPM2 protein expression after siRNA transfection. Cells were treated with siRNA targeting TRPM2 (si-TRPM2) or negative control siRNA (si-NC) for 48 hours, followed by immunoblotting with anti-TRPM2 antibody (1:1000 dilution). (B): Quantification of protein levels normalized to β-actin (ImageJ software); * indicates $p < 0.05$; ** indicates $p < 0.01$; one-way Anova with post-hoc Tukey test. (C) qPCR analysis of TRPM2 mRNA expression. Total RNA was reverse-transcribed into cDNA, and mRNA levels were measured using gene-specific primers (reference gene: GAPDH). Data were calculated by the $2^{-\Delta\Delta Ct}$ method; **** indicates$p < 0.0001$; one-way Anova with post-hoc Tukey test. Figure S2. H_2O_2activation of TRPM2 channels causes a rise in cytosolic level of $Ca^{2+}$and Zn^{2+}in DU145 cells. (A) DU145 cells were treated without (CTRL) or with H_2O_2 (100 μM) minus or plus ACA (2.5 μM), Clotrimazole (10 μM) and Econazole (10 μM). The cells were loaded with Fluo4-AM and analyzed by ImageJ; representative confocal images are shown; scale bars = 20 μm. (B) Mean ± SEM of average Ca^{2+} fluorescence per cell (CTRL: 120 cells; H_2O_2: 122 cells; ACA: 131 cells; Clotrimazole: 124 cells; Econazole: 128 cells) from three independent experiments performed as in (A); **** indicates $p < 0.0001$; one-way Anova, with post-hoc Tukey test. (C) DU145 cells were treated without (CTRL) or with H_2O_2 (100 μM) minus or plus ACA (2.5 μM), Clotrimazole (10 μM) and Econazole (10 μM). The cells were loaded with Fluozin-3-AM and analyzed by ImageJ; representative confocal images are shown; scale bars = 20 μm. (D) Mean ± SEM of average Zn^{2+} fluorescence per cell (CTRL: 112 cells; H_2O_2: 119 cells; ACA: 123 cells; Clotrimazole: 127 cells; Econazole: 133 cells) from three independent experiments performed as in (C); **** indicates $p < 0.0001$; one-way Anova, with post-hoc Tukey test. Figure S3. Zn^{2+}, rather than Ca^{2+}, mediates H_2O_2-induced actin remodelling in DU145 cells. (A) DU145 cells were either not treated (CTRL) or treated with H_2O_2 (100 μM) plus or minus BAPTA-AM (10 μM) and TPEN (5 μM) and then stained for F-actin. Representative images are shown; scale bars = 20 μm. (B) Mean ± SEM of filopodia number (5 cells) from three independent experiments performed as in (A); **** indicates $p < 0.0001$; one-way Anova with post-hoc Tukey test. (C) F-actin was stained following buffer (CTRL), A23187 (3 μM) minus or plus BAPTA-AM (10 μM) and Zn-PTO (3 μM) minus or plus TPEN (5 μM) treatments. Representative images are shown; scale bars = 20 μm. (D) Mean ± SEM of filopodia number (5 cells) from three independent experiments performed as in (C); *** indicates $p< 0.001$; **** indicates $p < 0.0001$. Figure S4. TRPM2 mediates palmitate-induced actin remodelling in DU145 cells. (A) DU145 cells were either not treated (CTRL) or treated with palmitate (500 μM) plus or minus NAC (10mM), ACA (2.5 μM), Clotrimazole (10 μM) and Econazole (10 μM) and then stained for F-actin. Representative images are shown; scale bars = 20 μm. (B) Mean ± SEM of Lamellipodia extent (5 cells) from three independent experiments performed as in (A); ** indicates $p< 0.01$; *** indicates $p < 0.001$; one-way Anova with post-hoc Tukey test. Figure S5 Palmitateactivation of TRPM2 channels causes a rise in cytosolic level of Ca^{2+} and Zn^{2+}in DU145

cells. (A) DU145 cells were treated without (CTRL) or with palmitate (500 μM) minus or plus ACA (2.5 μM), Clotrimazole (10 μM) and Econazole (10 μM). The cells were loaded with Fluo4-AM and analyzed by ImageJ; representative confocal images are shown; scale bars = 20 μm. (B) Mean ± SEM of average Ca^{2+} fluorescence per cell (CTRL: 117 cells; H_2O_2: 114 cells; ACA: 122 cells; Clotrimazole: 124 cells; Econazole: 123 cells) from three independent experiments performed as in (A); **** indicates $p < 0.0001$; one-way Anova, with post-hoc Tukey test. (C) DU145 cells were treated without (CTRL) or with palmitate (500 μM) minus or plus ACA (2.5 μM), Clotrimazole (10 μM) and Econazole (10 μM). The cells were loaded with Fluozin-3-AM and analyzed by ImageJ; representative confocal images are shown; scale bars = 20 μm. (D) Mean ± SEM of average Zn^{2+} fluorescence per cell (CTRL: 115 cells; H_2O_2: 110 cells; ACA: 121 cells; Clotrimazole: 122 cells; Econazole: 119 cells) from three independent experiments performed as in (C); **** indicates $p < 0.0001$; one-way Anova, with post-hoc Tukey test.

Supplementary Material 2.

Acknowledgements
We are grateful for Professor Wei Yang from Zhejiang University for helpful discussion on this project.

Authors' contributions
P. Q., J. Z., H. Z and X. L. performed the experiment. Q. Y. analyzed the data. F. L. drafted the paper. J. N. discussed and revised the manuscript. X. Y and F.L. contributed to the final approval of the manuscript.

Funding
This work was supported by grants from the Natural Science Foundation of China (31701211), Zhejiang Medical Health Science and Technology Project (2025 KY661) and the key research and development program of Ningxia Hui Autonomous Region (2019BFH02003).

Data availability
Data is provided within the manuscript or supplementary information files.

Declarations

Ethics approval and consent to participate
Not applicable.

Consent for publication
Not applicable.

Competing interests
The authors declare no competing interests.

Author details
[1]Department of Rehabilitation Medicine, Center for Rehabilitation Medicine, Rehabilitation & Sports Medicine Research Institute of Zhejiang Province, Zhejiang Provincial People's Hospital, Affiliated People's Hospital, Hangzhou Medical College, Hangzhou, China. [2]Department of Biophysics, Zhejiang University School of Medicine, Hangzhou, China. [3]Ningxia Key Laboratory of Craniocerebral Diseases, School of Pharmaceutical Sciences and School of Basic Medical Sciences, Ningxia Medical University, Yinchuan 750004, China.

Received: 16 July 2024 Accepted: 14 May 2025
Published online: 28 May 2025

References

1. Ridley AJ, et al. Cell migration: integrating signals from front to back. Science. 2003;302:1704–9.
2. Li L, He Y, Zhao M, Jiang J. Collective cell migration: Implications for wound healing and cancer invasion. Burns Trauma. 2013;1:21–6.
3. Gardel ML, Schneider IC, Aratyn-Schaus Y, Waterman CM. Mechanical integration of actin and adhesion dynamics in cell migration. Annu Rev Cell Dev Biol. 2010;26:315–33.
4. Mattila PK, Lappalainen P. Filopodia: molecular architecture and cellular functions. Nat Rev Mol Cell Biol. 2008;9:446–54.
5. Small JV, Stradal T, Vignal E, Rottner K. The lamellipodium: where motility begins. Trends Cell Biol. 2002;12:112–20.
6. Tojkander S, Gateva G, Lappalainen P. Actin stress fibers–assembly, dynamics and biological roles. J Cell Sci. 2012;125:1855–64.
7. Yamaguchi H, Condeelis J. Regulation of the actin cytoskeleton in cancer cell migration and invasion. Biochim Biophys Acta. 2007;1773:642–52.
8. Ben Mahdi MH, Andrieu V, Pasquier C. Focal adhesion kinase regulation by oxidative stress in different cell types. IUBMB Life. 2000;50:291–9.
9. Taulet N, Delorme-Walker VD, DerMardirossian C. Reactive oxygen species regulate protrusion efficiency by controlling actin dynamics. PLoS One. 2012;7:e41342.
10. Bhatt A, Kaverina I, Otey C, Huttenlocher A. Regulation of focal complex composition and disassembly by the calcium-dependent protease calpain. J Cell Sci. 2002;115:3415–25.
11. Oertner TG, Matus A. Calcium regulation of actin dynamics in dendritic spines. Cell Calcium. 2005;37:477–82.
12. Binker MG, Binker-Cosen AA, Richards D, Oliver B, Cosen-Binker LI. EGF promotes invasion by PANC-1 cells through Rac1/ROS-dependent secretion and activation of MMP-2. Biochem Biophys Res Commun. 2009;379:445–50.
13. Cho KH, et al. A ROS/STAT3/HIF-1alpha signaling cascade mediates EGF-induced TWIST1 expression and prostate cancer cell invasion. Prostate. 2014;74:528–36.
14. Nomura DK, et al. Monoacylglycerol lipase regulates a fatty acid network that promotes cancer pathogenesis. Cell. 2010;140:49–61.
15. Gellert M, Hanschmann EM, Lepka K, Berndt C, Lillig CH. Redox regulation of cytoskeletal dynamics during differentiation and de-differentiation. Biochim Biophys Acta. 2015;1850:1575–87.
16. Xu Q, Huff LP, Fujii M, Griendling KK. Redox regulation of the actin cytoskeleton and its role in the vascular system. Free Radic Biol Med. 2017;109:84–107.
17. Tochhawng L, Deng S, Pervaiz S, Yap CT. Redox regulation of cancer cell migration and invasion. Mitochondrion. 2013;13:246–53.
18. Currie E, Schulze A, Zechner R, Walther TC, Farese RV Jr. Cellular fatty acid metabolism and cancer. Cell Metab. 2013;18:153–61.
19. Tsai FC, et al. A polarized Ca2+, diacylglycerol and STIM1 signalling system regulates directed cell migration. Nat Cell Biol. 2014;16:133–44.
20. Naffa R, et al. The plasma membrane Ca(2+) pump PMCA4b regulates melanoma cell migration through remodeling of the actin cytoskeleton. Cancers (Basel). 2021;13:1354.
21. Sumoza-Toledo A, Penner R. TRPM2: a multifunctional ion channel for calcium signalling. J Physiol. 2011;589:1515–25.
22. Takahashi N, Kozai D, Kobayashi R, Ebert M, Mori Y. Roles of TRPM2 in oxidative stress. Cell Calcium. 2011;50:279–87.
23. Li FF, Munsey TS, Sivaprasadarao A. TRPM2-mediated rise in mitochondrial Zn promotes palmitate-induced mitochondrial fission and pancreatic β-cell death in rodents. Cell Death Differ. 2017;24:1999–2012.
24. Manna PT, et al. TRPM2-mediated intracellular Zn2+ release triggers pancreatic beta-cell death. Biochem J. 2015;466:537–46.
25. Li F, Abuarab N, Sivaprasadarao A. Reciprocal regulation of actin cytoskeleton remodelling and cell migration by Ca2+ and Zn2+: role of TRPM2 channels. J Cell Sci. 2016;129:2016–29.
26. Wiggins H, Rappoport J. An agarose spot assay for chemotactic invasion. Biotechniques. 2010;48:121–4.
27. Bohil AB, Robertson BW, Cheney RE. Myosin-X is a molecular motor that functions in filopodia formation. Proc Natl Acad Sci U S A. 2006;103:12411–6.
28. Xie Y, et al. Breast cancer migration and invasion depend on proteasome degradation of regulator of G-protein signaling 4. Cancer Res. 2009;69:5743–51.
29. Wang Q, et al. Mechanistic study of TRPM2-Ca(2+)-CAMK2-BECN1 signaling in oxidative stress-induced autophagy inhibition. Autophagy. 2016;12:1340–54.
30. Lange I, et al. TRPM2 functions as a lysosomal Ca2+-release channel in beta cells. Sci Signal. 2009;2:ra23.

31. Sumoza-Toledo A, et al. Dendritic cell maturation and chemotaxis is regulated by TRPM2-mediated lysosomal Ca2+ release. FASEB J. 2011;25:3529–42.
32. Zhang H, et al. The discovery of novel ACA derivatives as specific TRPM2 inhibitors that reduce ischemic injury both in vitro and in vivo. J Med Chem. 2021;64:3976–96.
33. Hill K, McNulty S, Randall AD. Inhibition of TRPM2 channels by the antifungal agents clotrimazole and econazole. Naunyn Schmiedebergs Arch Pharmacol. 2004;370:227–37.
34. Yu P, et al. A cell permeable NPE caged ADP-ribose for studying TRPM2. PLoS One. 2012;7:e51028.
35. Yang W, et al. Zinc inactivates melastatin transient receptor potential 2 channels via the outer pore. J Biol Chem. 2011;286:23789–98.
36. Nakamura S, et al. Palmitate induces insulin resistance in H4IIEC3 hepatocytes through reactive oxygen species produced by mitochondria. J Biol Chem. 2009;284:14809–18.
37. Morgan D, et al. Glucose, palmitate and pro-inflammatory cytokines modulate production and activity of a phagocyte-like NADPH oxidase in rat pancreatic islets and a clonal beta cell line. Diabetologia. 2007;50:359–69.
38. Liu LZ, et al. The activated CD36-Src axis promotes lung adenocarcinoma cell proliferation and actin remodeling-involved metastasis in high-fat environment. Cell Death Dis. 2023;14:548.
39. Belrose JC, Jackson MF. TRPM2: a candidate therapeutic target for treating neurological diseases. Acta Pharmacol Sin. 2018;39:722–32.
40. Diaz B, et al. Tks5-dependent, nox-mediated generation of reactive oxygen species is necessary for invadopodia formation. Sci Signal. 2009;2:ra53.
41. Lohmann C, Finski A, Bonhoeffer T. Local calcium transients regulate the spontaneous motility of dendritic filopodia. Nat Neurosci. 2005;8:305–12.
42. Wang Q, et al. A novel role for Wnt/Ca2+ signaling in actin cytoskeleton remodeling and cell motility in prostate cancer. Plos One. 2010;5:e10456.
43. Anson KJ, Corbet GA, Palmer AE. Zn(2+) influx activates ERK and Akt signaling pathways. Proc Natl Acad Sci U S A. 2021;118:e2015786118.
44. Mendoza MC, Vilela M, Juarez JE, Blenis J, Danuser G. ERK reinforces actin polymerization to power persistent edge protrusion during motility. Sci Signal. 2015;8:ra47.
45. Tektemur A, et al. TRPM2 mediates disruption of autophagy machinery and correlates with the grade level in prostate cancer. J Cancer Res Clin. 2019;145:1297–311.
46. Zeng X, et al. Novel role for the transient receptor potential channel TRPM2 in prostate cancer cell proliferation. Prostate Cancer Prostatic Dis. 2009;13:195–201.
47. Almasi S, et al. TRPM2 ion channel promotes gastric cancer migration, invasion and tumor growth through the AKT signaling pathway. Sci Rep. 2019;9:4182.
48. Bao L, et al. The human ion channel TRPM2 modulates migration and invasion in neuroblastoma through regulation of integrin expression. Sci Rep. 2022;12:20544.
49. Monteith GR, Prevarskaya N, Roberts-Thomson SJ. The calcium-cancer signalling nexus. Nat Rev Cancer. 2017;17:367–80.
50. Silvestri R, Nicoli V, Gangadharannambiar P, Crea F, Bootman MD. Calcium signalling pathways in prostate cancer initiation and progression. Nat Rev Urol. 2023;20:524–43.
51. Yang SY, Zhang JJL, Huang XY. Orai1 and STIM1 are critical for breast tumor cell migration and metastasis. Cancer Cell. 2009;15:124–34.
52. Grolez GP, et al. TRPM8 as an anti-tumoral target in prostate cancer growth and metastasis dissemination. Int J Mol Sci. 2022;23:6672.
53. Fabian A, et al. TRPC1 channels regulate directionality of migrating cells. Pflug Arch Eur J Phy. 2008;457:475–84.
54. Kagara N, Tanaka N, Noguchi S, Hirano T. Zinc and its transporter ZIP10 are involved in invasive behavior of breast cancer cells. Cancer Sci. 2007;98:692–7.
55. Taylor KM, et al. Zinc transporter ZIP10 forms a heteromer with ZIP6 which regulates embryonic development and cell migration. Biochem J. 2016;473:2531–44.
56. Sagredo AI, et al. TRPM4 channel is involved in regulating epithelial to mesenchymal transition, migration, and invasion of prostate cancer cell lines. J Cell Physiol. 2019;234:2037–50.
57. Heiden MGV, Cantley LC, Thompson CB. Understanding the warburg effect: the metabolic requirements of cell proliferation. Science. 2009;324:1029–33.
58. Yu J, et al. Hyperglycemia induces gastric carcinoma proliferation and migration via the Pin1/BRD4 pathway. Cell Death Discov. 2022;8:224.
59. Altea-Manzano P, et al. A palmitate-rich metastatic niche enables metastasis growth via p65 acetylation resulting in pro-metastatic NF-κB signaling. Nature cancer. 2023;4(3):344–64.
60. Nath A, et al. Palmitate-induced IRE1-XBP1-ZEB signaling represses desmoplakin expression and promotes cancer cell migration. Mol Cancer Res. 2021;19:240–8.
61. Xu S, et al. Palmitate induces ER calcium depletion and apoptosis in mouse podocytes subsequent to mitochondrial oxidative stress. Cell Death Dis. 2015;6:e1976.

Publisher's Note